Proceedings of The Thirteenth (2003) International Offshore and Polar Engineering Conference
Honolulu, Hawaii, USA, May 25−30, 2003

ISBN 1−880653-60−5 (Set); ISSN 1098−6189 (Set)

Numerical Analysis of the Internal Kinematics and Dynamics of Three-dimensional Breaking Waves on Slopes

B. Biausser, S.T. Grilli, P. Fraunié

LSEET, Université de Toulon et du Var / Principia R.D, La Garde / La Ciotat, France

Dpt. of ocean Engineering, University of Rhode Island, Narragansett, RI, USA

LSEET, Université de Toulon et du Var, La Garde , France

ABSTRACT

In this paper, we describe the breaking and post-breaking in a three-dimensional numerical wave tank of a solitary wave over a sloping ridge. The numerical model is based on coupling a higher-order Boundary Element Method (BEM) solution of fully nonlinear potential flow equations to a Volume Of Fluid (VOF) method solving Navier-Stokes or Euler equations, in three-dimensions (3D). The BEM solution is used as an initialization of the VOF/Navier-Stokes solver. Analysis of wave profiles and kinematics (velocity, vorticity, pressure) are carried out.

Keyword: breaking ocean waves; nonlinear surface waves; Boundary Element Method; Segment Lagrangian Volume of Fluid Method; numerical wave tank; three-dimensional flows.

INTRODUCTION

Over the past two decades many studies have been carried out to achieve a better understanding of ocean wave breaking. The study of breaking waves is of importance in many applications, such that air-sea interactions, sediment transport, or to understand damages caused to ocean and naval structures. Among the different types of breaking waves, we are interested here in three-dimensional (3-D) plunging breakers, characterised by the formation of a prominent jet in shallow water, whose dynamics and kinematics are not yet fully understood.

Most of the numerical studies dealing with breaking waves have been carried out for two-dimensional (2-D) problems. Hence, only a few results are available for fully three-dimensional (3-D) breakers. In the present paper, the breaking of an incident solitary wave over a sloping ridge is investigated. To do so, two numerical methods are coupled, namely a Boundary Integral Equation method (BIEM) for the wave propagation and shoaling stages, and a Volume Of Fluid (VOF) method combined with a Navier-Stokes (or currently Euler) solver, for the breaking stage.

The higher-order 3D-BIEM model of Grilli et al. (2001), which solves fully non-linear potential flow equations, is very accurate and efficient for modeling wave shoaling and the initial stages of wave overturning, but is unable to deal with interface reconnection when breaking occurs.

The VOF interface tracking method is less numerically accurate and much more computationally intensive than the BIEM model for wave shoaling, but it allows to simulate breaking and post-breaking stages. Moreover, after breaking occurs, the flow becomes rotational so that potential theory becomes invalid. This is the reason why the coupling between the BIEM and VOF/Navier-Stokes solver is achieved. The pre-breaking phase is computed with the BIEM method, whereas the breaking and post-breaking phases are computed using the VOF method, thus combining the advantages of both methods.

The paper is organized as follows. The first section deals with mathematical formulation. In the second section the numerical models are briefly presented. Note that more details on numerical methods are given in a companion paper (Biausser, et al., 2003). Finally, the case of a solitary wave overturning and breaking over a sloping bottom is analyzed in the last section.

MATHEMATICAL FORMULATION

BIEM formulation

Equations for fully nonlinear potential flows with a free surface are listed below. The velocity potential $\phi(\mathbf{x},t)$ is introduced to describe inviscid irrotational 3D flows, in Cartesian coordinates $\mathbf{X}=(x,y,z)$, with z the vertical upward direction ($z = 0$ at the undisturbed free surface), and the fluid velocity is expressed as $\mathbf{u} = \nabla\phi$. Continuity equation in the fluid domain $\Omega(t)$ with boundary $\Gamma(t)$ is Laplace's equation

$$\nabla^2 \phi = 0. \tag{1}$$

The corresponding three-dimensional free-space Green's function is defined as

$$G(\mathbf{x},\mathbf{x}_1) = \frac{1}{4\pi r} \qquad \text{with} \qquad \frac{\partial G}{\partial n}(\mathbf{x},\mathbf{x}_1) = -\frac{1}{4\pi}\frac{\mathbf{r.n}}{r^3}, \tag{2}$$

with, $r = |\mathbf{X} - \mathbf{X}_1|$ the distance from the source point $\mathbf{X}$ to the field point $\mathbf{X}_1$ (both on boundary Γ), and $\mathbf{n}$ the outward unit vector normal to the boundary at point $\mathbf{X}$.

Green's second identity transforms Eq. (1) into the Boundary Integral Equation (BIE)

$$\alpha(\mathbf{x}_l)\phi(\mathbf{x}_l) = \int_\Gamma \left[\frac{\partial \phi}{\partial n}(\mathbf{x}) G(\mathbf{x}, \mathbf{x}_l) - \phi(\mathbf{x}) \frac{\partial G}{\partial n}(\mathbf{x}, \mathbf{x}_l) \right] d\Gamma , \quad (3)$$

The boundary is divided into various parts in which different boundary conditions are specified. On the free surface $\Gamma_f(t)$, ϕ satisfies the nonlinear kinematic and dynamic boundary conditions,

$$\frac{D\mathbf{R}}{Dt} = \mathbf{u} = \nabla\phi \quad , \quad (4)$$

$$\frac{D\phi}{Dt} = -gz + \frac{1}{2}\nabla\phi.\nabla\phi - \frac{p}{\rho} \ , \quad (5)$$

respectively, in a Mixed Eulerian-Lagrangian formulation (MEL), with **R** the position vector of a fluid particle on the free surface, g the acceleration due to gravity, p the atmospheric pressure, ρ the fluid density and $D/Dt = \partial/\partial t + \nabla\phi.\nabla$ the Lagrangian time derivative. The effects of surface tension are neglected.

For simple waves, such as solitary waves, the free surface shape, potential and normal velocity of the incident wave are specified at time $t = 0$ on the free surface based on Tanaka's method (Tanaka,1986). More complex incident wave conditions can be specified using numerical wavemakers (e.g., Grilli and Horrillo, 1997, 1999; Brandini and Grilli, 2001).

On the bottom boundary, Γ_b and on other fixed parts of the boundary, a no-flow condition is prescribed as

$$\frac{\partial \phi}{\partial n} = 0. \quad (6)$$

Once the BIE (3) is solved, the solution within the domain can be explicitly calculated, based on boundary values. Using Eq. (3), for instance, the internal velocity at the interior point $\mathbf{X}_i$ is given by Eqs. (7) and (8), respectively, below

$$\mathbf{u}(\mathbf{x}_i) = \nabla\phi(\mathbf{x}_i) = \int_\Gamma \left[\frac{\partial \phi}{\partial n}(\mathbf{x}) Q(\mathbf{x}, \mathbf{x}_i) - \phi(\mathbf{x}) \frac{\partial Q}{\partial n}(\mathbf{x}, \mathbf{x}_i) \right] d\Gamma , \quad (7)$$

$$Q(\mathbf{x}, \mathbf{x}_i) = \frac{1}{4\pi r^3}\mathbf{r} \ , \ \frac{\partial Q}{\partial n}(\mathbf{x}, \mathbf{x}_i) = \frac{1}{4\pi r^3}\left[\mathbf{n} - 3(\mathbf{r}.\mathbf{n})\frac{\mathbf{r}}{r} \right] , \quad (8)$$

where r denotes the distance from the boundary point **X** to $\mathbf{X}_i$.

Navier-Stokes Formulation

The 3D Navier-Stokes equations for two-phase (air-water) flows are given as follows, in a semi-conservative curvilinear formulation:

$$\frac{1}{J}\frac{\partial W}{\partial t} + \frac{\partial F}{\partial \xi} + \frac{\partial G}{\partial \eta} + \frac{\partial H}{\partial \chi} = \frac{R}{J} + \frac{T}{J} \quad (9)$$

where F, G and H are flux terms, R is the volumetric force source term and T the surface tension source term, with :

$$F = \frac{1}{J}\begin{pmatrix} \rho\tilde{u} \\ \rho\tilde{u}u + \xi_x p - \vec{\nabla}(\xi).\vec{\tau}_x \\ \rho\tilde{u}v + \xi_y p - \vec{\nabla}(\xi).\vec{\tau}_y \\ \rho\tilde{u}w + \xi_z p - \vec{\nabla}(\xi).\vec{\tau}_z \end{pmatrix}; G = \frac{1}{J}\begin{pmatrix} \rho\tilde{v} \\ \rho\tilde{v}u + \eta_x p - \vec{\nabla}(\eta).\vec{\tau}_x \\ \rho\tilde{v}v + \eta_y p - \vec{\nabla}(\eta).\vec{\tau}_y \\ \rho\tilde{v}w + \eta_z p - \vec{\nabla}(\eta).\vec{\tau}_z \end{pmatrix};$$

$$H = \frac{1}{J}\begin{pmatrix} \rho\tilde{w} \\ \rho\tilde{w}u + \chi_x p - \vec{\nabla}(\chi).\vec{\tau}_x \\ \rho\tilde{w}v + \chi_y p - \vec{\nabla}(\xi).\vec{\tau}_y \\ \rho\tilde{w}w + \chi_z p - \vec{\nabla}(\xi).\vec{\tau}_z \end{pmatrix}; W = \begin{pmatrix} 0 \\ \rho u \\ \rho v \\ \rho w \end{pmatrix}; T = \begin{pmatrix} 0 \\ \sigma K n_x \\ \sigma K n_y \\ \sigma K n_z \end{pmatrix}; R = \begin{pmatrix} 0 \\ \rho f_x \\ \rho f_y \\ \rho f_z \end{pmatrix}$$

$$\tilde{u} = \xi_x u + \xi_y v + \xi_z w \, ; \, \tilde{v} = \eta_x u + \eta_y v + \eta_z w \, ; \, \tilde{w} = \chi_x u + \chi_y v + \chi_z w \, ;$$

$$J = \frac{\partial(\xi, \eta, \chi)}{\partial(x, y, z)}$$

$$\vec{\tau}_x = \vec{\bar{\tau}}.\vec{e}_x \quad \vec{\tau}_y = \vec{\bar{\tau}}.\vec{e}_y \quad \vec{\tau}_z = \vec{\bar{\tau}}.\vec{e}_z \quad \vec{\bar{\tau}} = \mu(\vec{\nabla}\vec{U} + \vec{\nabla}^t\vec{U}) \quad (10)$$

where (ξ, η, χ) denote curvilinear coordinates, J is the Jacobian matrix of the coordinate transformation, σ is the surface tension coefficient, K the surface curvature and $\vec{n} = (n_x, n_y, n_z)$ the normal vector to the interface. Additionally, (u,v,w) are the Cartesian velocity components for each phase, $(\tilde{u}, \tilde{v}, \tilde{w})$ the contravariant velocity components, p the pressure, ρ the density, μ the molecular viscosity, and $\vec{\bar{\tau}}$ the viscous stress tensor. Nevertheless, the viscosity will be neglected here.

NUMERICAL MODELS

For details, see our companion paper, Biausser et al. (2003).

Numerical method for the BIEM model

A second-order explicit scheme based on Taylor series expansions is used to update the position **R** and velocity potential ϕ on the free surface. A high-order Boundary Element Method (BEM) is used to solve numerically the BIEs for ϕ and $\partial\phi/\partial t$ (Grilli et al., 2001). The boundary is discretized into collocation nodes, defining two-dimensional elements for local interpolations of the solution in between these nodes. Within each element, the boundary geometry and field variables are interpolated using cubic polynomial shape functions (the boundary elements are 4X4-node quadrilaterals associated with bi-cubic shape functions of which only the middle quadrilateral is used). The discretized boundary integrals are evaluated for each collocation node by numerical integration. A special treatment is applied for weakly singular integrals. As the linear algebric system resulting from the discretization of the BIE (3) is in general dense and non-symmetric, a generalized minimal residual (GMRES) algorithm with preconditioning is used to solve it (Xü & Yue, 1992). Accuracy is increased in regions of high variability by redistributing nodes using a regridding technique based on the BEM shape functions.

Numerical method for the VOF/Navier-Stokes model

Time discretization for the Navier-Stokes model is ensured using a fully implicit second-order scheme. The solution of the non-linear system for the unknown values at step n+1 is based on the pseudo-compressibility method (Viviand 1980, De Jouëtte et al. 1991), in which a time-like

variable τ, called pseudo-time is introduced. Thus, in Eq. (9), we add pseudo-unsteady terms, which are derivatives of the unknowns at time level n+1, with respect to τ. These pseudo-density terms involve a new unknown $\tilde{\rho}$, called pseudo-density, which is constrained to remain positive. The pressure is calculated as a function of $\tilde{\rho}$, through an additional pseudo-state equation:

$$p^{n+1} = \rho(U_0^2 + \lambda U_n^2)\ln\left(\frac{\tilde{\rho}}{\rho}\right)^{n+1} \tag{11}$$

The choice of an optimal pseudo-state equation is discussed in Viviand (1995).

NUMERICAL RESULTS

In this section, the two numerical models described above are used together to compute the shoaling and breaking of a solitary wave over a sloping ridge. The BIEM model is used for the initial stage, in which most of the wave shoaling occurs. Laboratory experiments confirm that potential flow theory is very accurate to describe wave transformations at this stage (Grilli et al., 1994, 1997). When the wave is close to overturning, the BIEM solution is used to initialize the Navier-Stokes/VOF model, both for free surface/interface geometry and internal velocity and pressure fields at cell centers. The second part of the simulation i.e. overturning, breaking and post-breaking, is computed with the VOF method, by solving Euler equations (i.e., viscosity is neglected). [Note, this coupling procedure was successfully applied in 2D by Guignard et al. (1999). Also see Biausser et al. (2003).] The air phase dynamics is neglected in this case for computational time reasons.

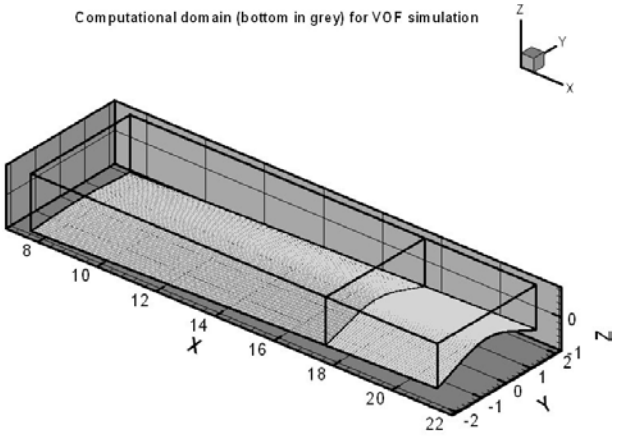

Figure 1: BIEM/VOF computational domain for solitary wave shoaling over a 3-D ridge

Computational domain

The domain has a flat bottom (with depth h_0 = 1 m), for x = 1 to 5.225 m, and a sloping ridge, starting at x=5.225 m, with a 1 : 15 slope in the middle cross-section (y = 0) and a transverse modulation of the form sech(ky) (y = ±2 m, k = 0.5), so that the bottom slope on the sides is 1 : 36 (Fig. 1). For the first part of the simulation (BIEM), the ridge is truncated at x = 17.6 m. Let H_0 be the initial height of the wave and $H_0'=H_0/h_0$. The initial wave is a numerically exact solitary wave (Tanaka, 1986), with H_0' = 0.6 and its crest initially located at x = 5.7 m. The wave is propagated for time, $t' = t\sqrt{g/h_0}$ = 0 to t' = 6. The VOF model is initialized for t' = 6 in the computational domain, for $x \in$ [7.6;21.3] using 352x40x64 computational cells (Fig. 1).

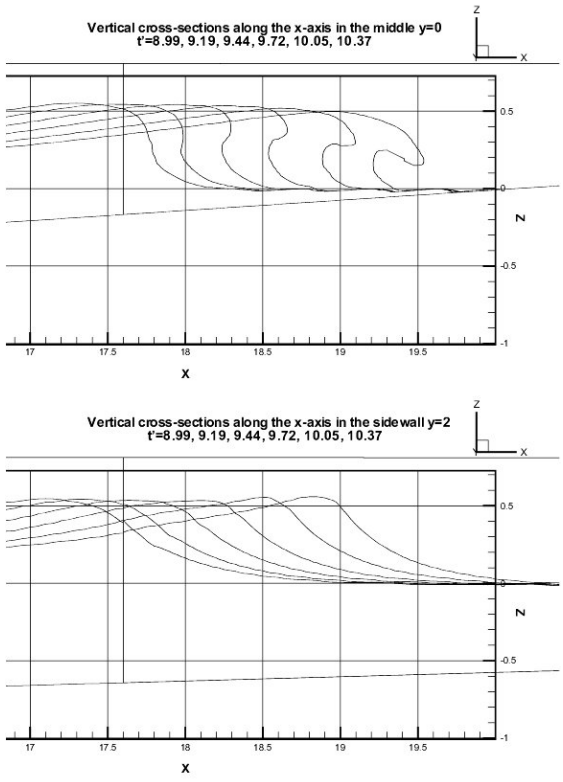

Figure 2: vertical cross-sections along the x-axis in y = 0 and y = ±2 for computations in computational domain of Fig. 1 of the shoaling of a solitary wave of initial height $H' \approx 0.6$.

Overturning stage

As wave shoaling continues in the VOF domain (Fig. 1), the bottom variation progressively leads to wave overturning. Fig. 2 displays vertical cross-sections of the free surface calculated in the middle (y=0) and at the sidewalls (y=±2 m) of the VOF computational domain, for times t' =8.99, 9.19, 9.44, 9.72, 10.05, 10.37. Full 3D views for times t' =9.19, 9.44, 9.72, 10.05 and 10.37 are presented on Fig. 3. The 3D aspect of wave overturning appears clearly on figures 2 and 3. Due to the depth variation over the ridge, one can see that the wave profile at y = 0 develops overturning, with a prominent jet, while the surface profile at y' = ±2 is still of moderate slope. The wave reaches its maximum height of $H' \approx 0.58$ near the breaking point. The surface elevation then gradually decreases as the jet of water is projected forward.

Another interesting analysis is to compare the pressure field at the breaking point to an hydrostatic pressure field based on surface elevation. This allows estimating the applicability of long waves models, which assume hydrostatic pressure. One can see on Fig. 4 that the ratio between computed pressure and hydrostatic pressure varies between 0.2 and 2.5, for the wave near the breaking point (vertical

tangent on the front face). The wave pressure field at the breaking point is clearly far from hydrostatic, especially just in front of the wave, due to large vertical accelerations (Guyenne and Grilli, 2002), neglected in long waves model.

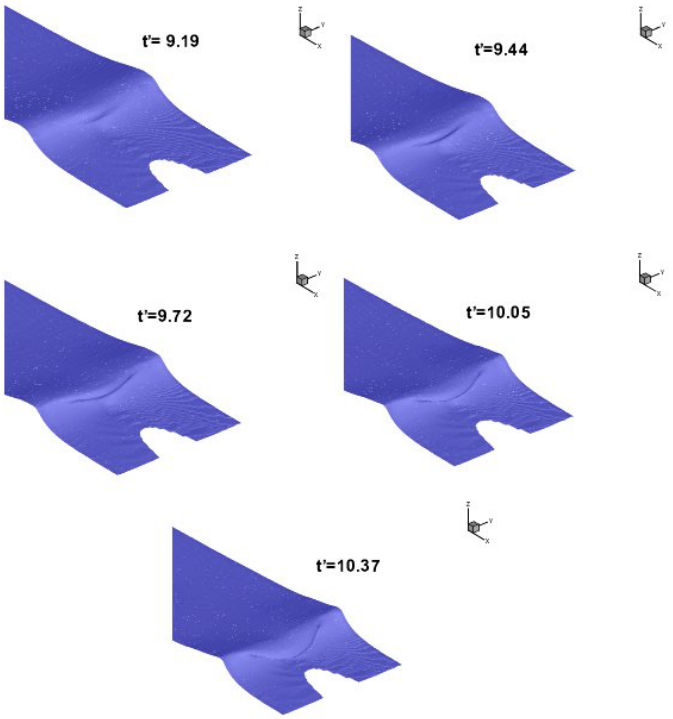

Figure 3 : details of 3-D overturning of the solitary wave of Fig. 2

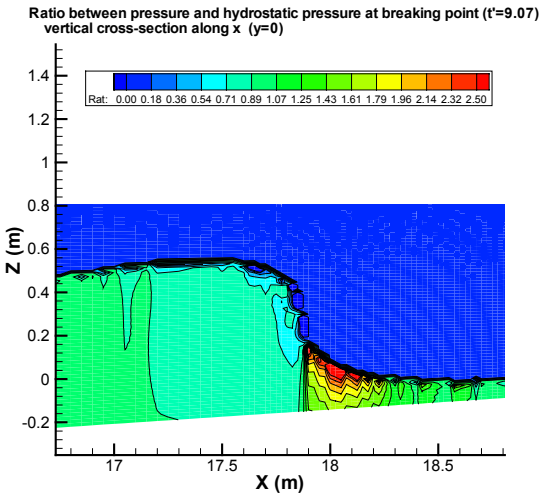

Figure 4: ratio between computed pressure and hydrostatic pressure for the breaking solitary wave of Fig. 2 ($y = 0$)

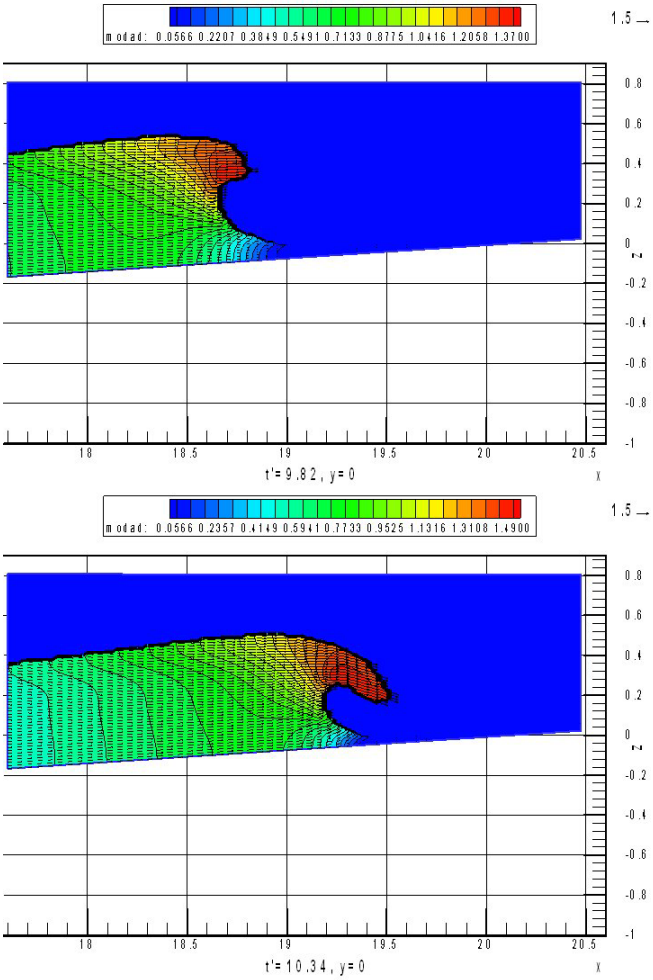

Figure 5: non-dimensional velocity field and magnitude at $t' = 9.82$ and $t' = 10.34$ ($y = 0$) for results of Figs. 2-4.

Figure 5 displays the non-dimensional internal velocity field and its non-dimensional magnitude, computed at $t' = 9.82$ and $t' = 10.34$ for $y = 0$, after the breaking point. During breaking, high velocities are observed to occur in the breaker jet, due to high flow convergence. The velocity increases and exhibits more variation in the vertical direction as one enters the breaker jet.

Figure 6 displays the transverse variations of the velocity, due to focusing of the flow by the ridge. Non-dimensional velocities and non-dimensional velocity magnitude are again shown for $t' = 9.82$ and $t' = 10.34$, at $z = -0.2$ m.

Breaking and post-breaking stages

Breaking occurs first at the centre of the ridge and then propagates progressively towards the sides. Fig. 7 displays the breaking for $t' = 10.53$, 10.68, 10.82 and 10.89 at the centre of the ridge. The breaker jet impacts the forward free surface at x= 19.85 m for time t'=10.65. The maximum non-dimensional velocity magnitude at this time is 1.63. The wave is submitted to a strong acceleration before breaking. The maximum acceleration magnitude is 4.9 g just before impact.

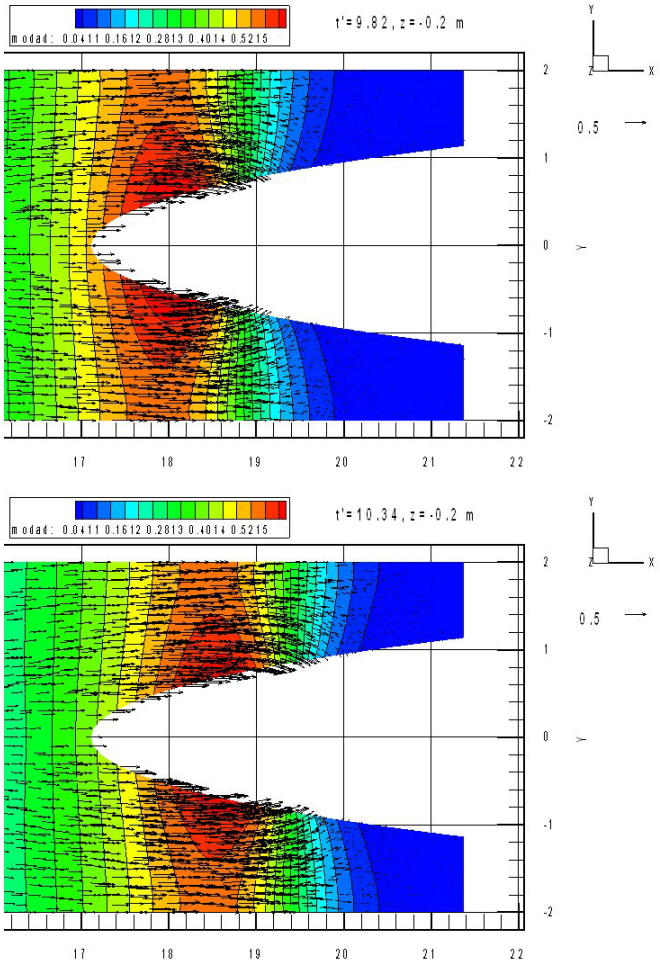

figure 6 : transverse modulation of the velocity (z = -0.2m) for the results of Figs. 2-5.

The 3-D aspects of breaking/post-breaking are shown on Fig. 8, where different vertical cross sections along the y-axis are displayed, and Fig. 9, where full 3-D views of breaking are shown. Initially, breaking occurs in the middle part of the wave but not yet on the side parts.

Figs. 10ab present the evolution of vorticity in the vertical cross-section at y = 0.4 m, for different non-dimensional times, before and after jet impact. As the impact of the breaker jet occurs in shallow water, only little generation of vorticity is observed. A model including viscosity should create more vorticity. Maximum vorticity is observed to occur at the impact location.

After impact, Fig. 11 shows that the air tube formed by the breaker is progressively crashed as the wave continues to collapse in the swash zone. The water jet is then projected with high velocity along the slope. After splash-up, no secondary jet is observed because breaking occurs in shallow water.

Numerical performances and comparisons with BIEM results

The CPU time for the VOF simulations was five days and ten hours, on a Digital Dec alpha 500MHz bi-processor. The numerical error on volume conservation was less than 0.7%. The error on total energy conservation was larger, about 10%. This can be explained by the single-phase flow modelling used in the VOF model, in which fields are interpolated on the free surface cells. In the case of a solitary wave, maximum velocities are located at the wave crest, precisely where interpolations are applied. This leads to (non-physical) loss of both wave energy and amplitude. This was also observed by Guignard et al. (1999, 2001), in 2-D computations.

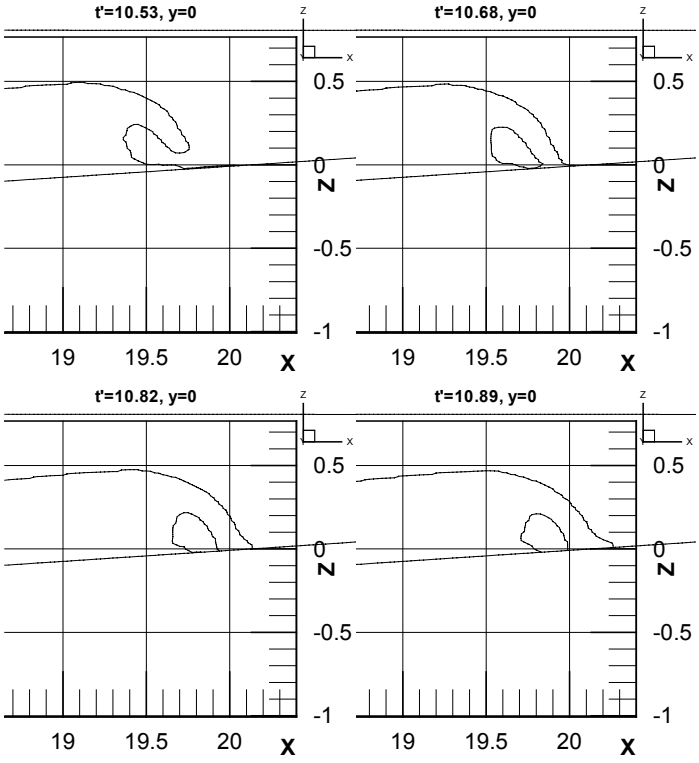

Figure 7 : breaking at the centre of the ridge breaking for t' = 10.53, 10.68, 10.82 and 10.89 (y= 0) for results of Figs. 2-6.

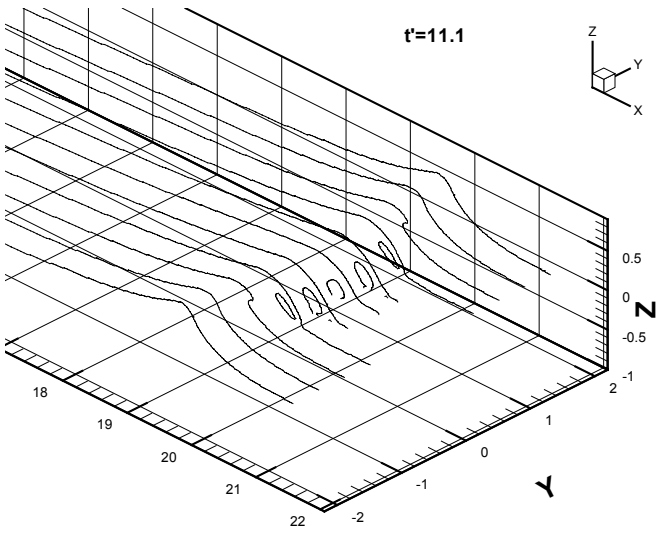

Figure 8 : breaking at t' = 11.01 for different vertical cross-sections along the x-axis in Figs. 2-7 results.

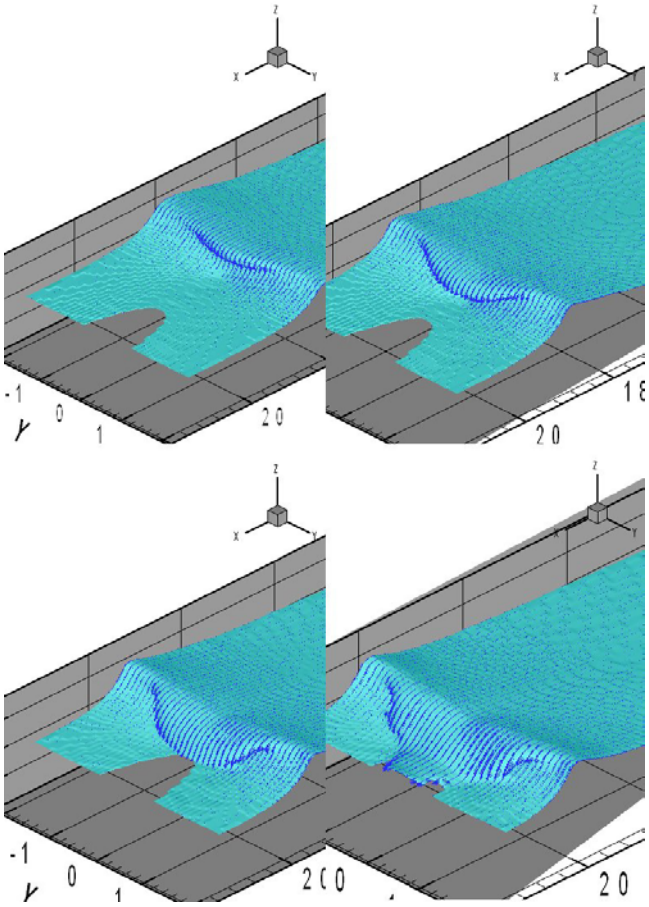

Figure 9: evolution of breaking (full 3-D view) for Figs. 2-8 results

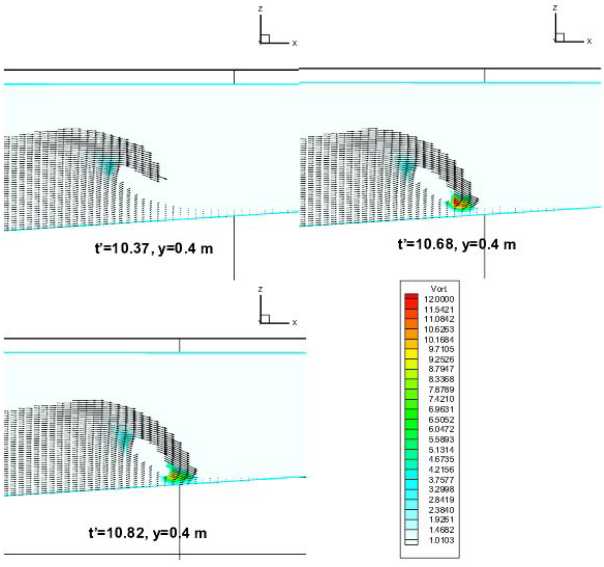

Figure 10.a: vorticity in the plane y = 0.4 m for different non-dimensional times t' in Figs. 2-9 results.

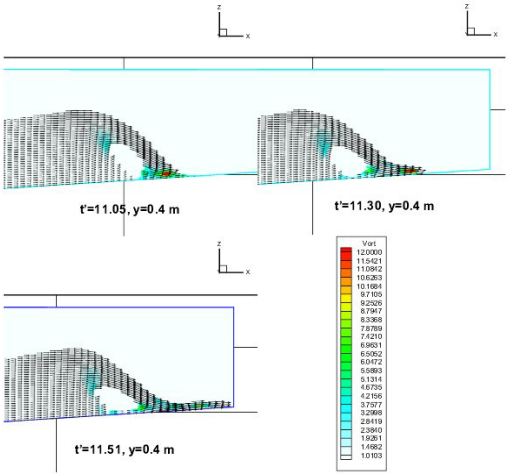

Figure 10.b: vorticity in the plane y = 0.4 m for different non-dimensional times t' in Figs. 2-9 results.

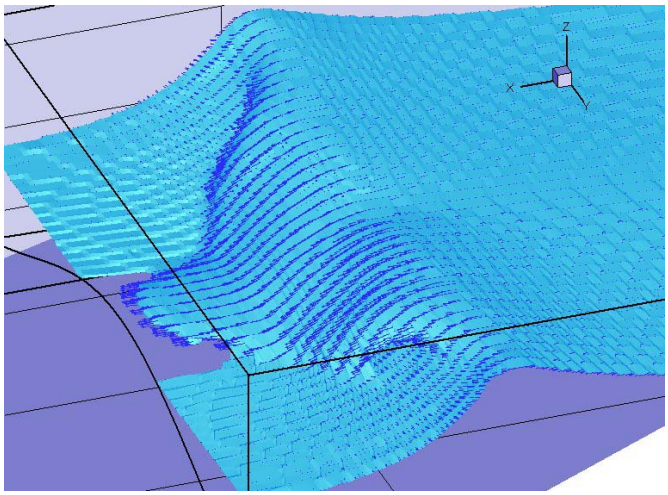

Figure 11: wave collapsing and beginning of the swash zone

The numerical loss of energy can also explain the delay observed for the onset of breaking in VOF results, with respect to BIEM results. Comparisons at t' = 9.182 and t' = 9.196 between VOF results and Guyenne and Grilli's BIEM results for y = 0 m and y = 2 m show that the wave height is larger with the BIEM. In Guyenne and Grilli's (2002) computations, reproduced in Fig. 12, wave energy was very precisely conserved and breaking occurred earlier (at $t' \approx 9$ and $x \approx 18$ m), than in the present computations. Wave height at breaking was also quite a bit larger, about 0.7 m (whereas it is 0.58 m in the present computations). Figure 12 also shows that the overturning stage is more developed for similar times in BIEM results. A more detailed comparison would show that the maximum computed velocity before impact is 1.63 in VOF results and 1.94 in BIEM results. The maximum acceleration at this stage is 4.9 g in VOF results and 5.9 g in BIEM results (Guyenne and Grilli, 2002). Thus, the wave motion is more dynamic and the computed velocities and accelerations are larger in BIEM results than with the Navier-Stokes/Euler solver. In addition to the advantage of using a more efficient and numerically accurate model, the lack of vorticity generated in the flow before jet impact (Fig.10) further supports the relevance of using potential flow theory to

model wave transformation up to near breaking with the BIEM model. Despite the differences discussed above, however, we see that, the wave general motion is similar with the two methods. The focusing on the ridge (especially the 3-D effects on transverse velocity), the dynamics and the aspect of the breaker jet are quite close.

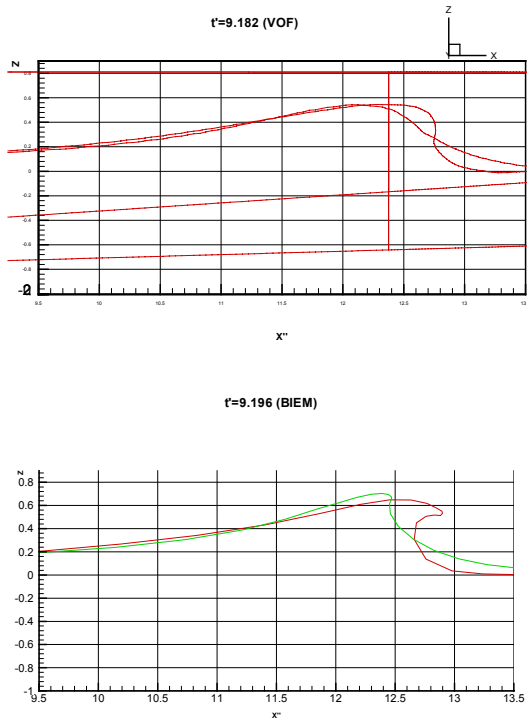

Figure 12 : comparisons between VOF results (above) and BIEM results (below), for similar t' and $y = 0$ m and $y = 2$ m

CONCLUSIONS

The coupling between BIEM and VOF methods has been used to successfully compute 3D overturning, (plunging) breaking and post-breaking stages of a large solitary wave over a sloping ridge with a lateral modulation. BIEM results computed close to breaking have been used to initialize the VOF method on a very refined grid, in which breaking and post-breaking stages, with interface reconnection, can be quite accurately computed.

Three-dimensional effects on wave profile and kinematics have been illustrated and discussed. Comparisons with late stages of BIEM computations before jet impact have shown that, despite a loss of amplitude and energy in the VOF model, the kinematics of the flow and general shape of the wave are consistent with those computed in the more accurate BIEM model.

Future improvements of the VOF model should include using viscosity (because only little vorticity is generated here after breaking), with a proper representation of dissipation at sub-grid scales. Although two-phase flows modelling is costly, boundary condition on the interface is taken into account in a better way. This should allow to reduce wave energy loss before breaking.

REFERENCES

Biausser, B., Guignard, S., Marcer, and R., Fraunié, P. (2001). "Numerical simulations of free surface flows using a new VOF method," *Proc. 4th Seminar Euler and Navier-Stokes Equations, Institute of Thermomechanics, Prague*.

Biausser, B., Guignard, S., Marcer, and R., Fraunié, P. (2002). (2001). "3-D two-phase flows numerical simulations by SL-VOF method", *submitted to Int. Jour. For Num. Meth. In Fluids.*

Biausser, B., Grilli, S.T. and Fraunié, P. (2003). "Numerical Simulations of Three-dimensional Wave Breaking by Coupling of a VOF Method and a Boundary Element Method", *Proc. 13th Offshore and Polar Engng. Conf.* (ISOPE03, Honolulu, HI, USA, May 2003), *submitted for publication.*.

Brandini, C. and S.T., Grilli (2001). "Modeling of freak wave generation in a 3D-NWT, " *In Proc. 11th Offshore and Polar Engng. Conf.* (ISOPE01, Stavanger, Norway, June 2001), Vol III, pp 124-131.

De Jouëtte, C., Viviand, H., Wornom, S. and Le Gouez, J.M. (1991). "Pseudo-Compressibility Methods for Incompressible Flow Calculation," *Proc 4th International Symposium on Computational Fluid Dynamics,University of California, Davis*.

Grilli, S.T., Guyenne, P. and Dias, F. (2001). "A fully nonlinear model forthree-dimensional overturning waves over arbitrary bottom," *Intl J. Numer. Meth. Fluids* , Vol 35, No 1, pp 829-867.

Grilli, S.T., and Subramanya, R (1996). "Numerical modeling of wave breaking induced by fixed or moving boundaries," *Computational Mech.*, Vol 17, pp 374-391.

Grilli, S., Subramanya, R., Svendsen, I.A. and Veeramony, J. (1994). "Shoaling of Solitary Waves on Plane Beaches*." J. Waterway Port Coastal and Ocean Engng.*, Vol 120, No 6, pp 609-628.

Grilli, S.T., Svendsen, I.A. and Subramanya, R. (1997). "Breaking Criterion and Characteristics for Solitary Waves on Slopes*." J. Waterway Port Coastal and Ocean Engng.*, Vol 123, No 3, pp 102-112.

Guignard, S., Grilli, S.T., Marcer, R. and Rey, V. (1999). "Computation of shoaling and breaking waves in nearshore areas by the coupling of BEM and VOF methods." In *Proc. 9th Offshore and Polar Engng. Conf.* (ISOPE99, Brest, France, May 1999), Vol. III, pp 304-309

Guignard, S., Marcer, R., Rey, V., Kharif, Ch. and Fraunié, P. (2001). "Solitary wave breaking on sloping beaches:2D two-phase flow numerical simulation by SL-VOF method". *Eur. J. Mech.*

Guyenne, P., and Grilli, S.T. (2002). "Numerical study of three-dimensional overturning waves in shallow water", *submitted for publication.*.

Hirt, C.W., and Nichols, B.D. (1981). "Volume Of Fluid Method for the dynamics of free boundaries," *J.Comp. Phys.,* Vol 39, pp 323-345.

Jameson, A., Schmidt, W. and Turkel, E. (1981). "Numerical solutions of Euler equations by finite volume methods using Runge-Kutta time stepping schemes," *AIAA Paper 81-1259*.

Tanaka, M. (1986). "The stability of solitary waves," *Phys. Fluids,* Vol 29*,* No 3*,* pp 650-655.

Viviand, H. (1980). "Pseudo-unsteady Methods for Transonic Flow Computations," *19th International Conference on Numerical Methods in Fluid Dynamics, Stanford, in Lecture Notes in Physics,* Vol. 141, Springer-Verlag, New-York.

Viviand, H. (1995). "Analysis of pseudo-compressibility systems for compressible and incompressible flows," *Comp. Fluid Dynamics Review,Hafez-Oshima editor, Wiley publishers,* pp.399-418.

Xü, H, and Yue, D.K.P. (1992). "Computations of fully nonlinear three-dimensional water waves," *Proc. 19th Symp. On Naval Hydrodynamics, Seoul, Korea.*

ACKNOWLEDGEMENT

The authors wish to acknowledge support from the French National Program PATOM (Programme Atmosphère et Océan à Multiéchelles).